

## Kinetic Divertor Modeling

F. Taccogna<sup>1</sup>, P. Minelli<sup>1</sup>, D. Bruno<sup>1</sup>

<sup>1</sup>*Istituto di Metodologie Inorganiche e dei Plasmi (IMIP), Consiglio Nazionale delle Ricerche,  
via Amendola 122/D - 70126 Bari (Italy)*

The cold divertor is considered to be the most reliable concept in Tokamak reactors for an adequate reduction of plasma power flux deposited on the plate. This is mainly achieved by recombination mechanisms [1]. From this point of view, the coupling between plasma and neutrals is a fundamental aspect in divertor modeling. In fact, electron and proton reactions with vibrationally excited molecules  $H_2(v)$  lead to plasma volumetric recombination by the so called molecular assisted recombination (MAR) chains [2]:

- negative-ion mediated recombination:  $e + H_2(v) \rightarrow H + H^-$ ,  $H^- + H^+ \rightarrow H + H$
- molecular-ion mediated recombination:  $H^+ + H_2(v) \rightarrow H + H_2^+$ ,  $H_2^+ + e \rightarrow H + H$

which are more important than the direct electron-ion (radiative and three-body) recombination mechanisms (EIR). In addition, particle-surface interaction (in particular vibrational relaxation and associative desorption) could further increase the efficiency of MAR reactions by production of vibrational excited molecules from the wall.

Collisional-radiative (CR) [3-6] and fluid models [7-9] used for analysis of divertor plasmas are not suitable to describe this scenario. These models are usually based on the rate balance master equations and the particle dynamics and gas-wall interaction are not well represented. Excited states with large decay time (like the vibrational states of molecules) cannot be treated in the local CR approximation. For this reason, in this work, we have developed a 1D [the simulation domain is bounded between the plasma bulk (left side) and the divertor plate (right side)] electrostatic Particle-in-Cell (PIC) [10] coupled with a Direct Simulation Monte Carlo (DSMC) [11] model. The motion of charged particles (electrons and ions  $H^+$ ,  $H_2^+$  and  $H^-$ ) in their self-consistent electric field (a fixed tilted magnetic field  $B=1$  T is imposed) and of neutral-particle states [ $H(n=1,2,3)$  and  $H_2(X^1\Sigma_g^+, v=0, \dots, 14)$ ] is simulated iteratively coupling plasma and neutral dynamics. Collisional volumetric (see Table I for the complete list) and surface emission (see Table II for the complete list) processes have been included by using different Monte Carlo techniques [12-14].

**Table I** - List of the most significant volume processes included in the model.

Coll. species	Processees	Reaction Formulas
e	1) e-induced atomic elastic / electronic excit.	$e + H(n) \leftrightarrow e + H(m)$
	2) e-induced atomic ionization	$e + H(n) \rightarrow 2e + H^+$
	3) e-induced vibrational excitation eV	$e + H_2(v) \leftrightarrow e + H_2(w)$
	4) e-induced vibrational excitation EV	$e + H_2(v) \rightarrow e + H_2(w) + hv$
	5) e-induced molecular ionization	$e + H_2(v) \rightarrow 2e + H_2^+$
	6) e-induced dissociation	$e + H_2(v) \rightarrow e + H(n=1) + H(n=2,3)$
	7) e-induced dissociative ionization	$e + H_2(v) \rightarrow 2e + H + H^+$
	8) e-induced molecular electronic excitation	$e + H_2(v) \rightarrow e + H_2^*$
	9) electron dissociative attachment	$e + H_2(v) \rightarrow H + H^-$
$H^+$	10) p-induced atomic elastic	$H^+ + H(n) \leftrightarrow H^+ + H(n)$
	11) p-induced atomic charge exchange	$H^+ + H(n) \rightarrow H(n=2) + H^+$
	12) p-induced elastic/vibrational excitation	$H^+ + H_2(v) \leftrightarrow H^+ + H_2(w)$
	13) atomic-to-molecular ion conversion	$H^+ + H_2(v) \rightarrow H_2^+ + H(n=1)$
$H_2^+$	14) p-induced dissociation	$H^+ + H_2(v) \rightarrow H^+ + H(n=1) + H(n=1)$
	15) molecular-to-atom ion conversion	$H_2^+ + H(n=1) \rightarrow H^+ + H_2(v=1,8)$
	16) charge exchange with molecule	$H_2^+ + H_2(v) \rightarrow H_2(w) + H_2^+$
$H^-$	17) p2-induced dissociation	$H_2^+ + H_2(v) \rightarrow H^+ + H(n=1) + H_2(v)$
	18) electron associative detachment with atom	$H^- + H(n) \rightarrow H_2(v) + e$
	19) electron non associat. detachment with atom	$H^- + H(n) \rightarrow H(n=2) + H(n) + e$
	20) negative ion charge exchange	$H^- + H(n) \rightarrow H(n=2) + H^-$
Plas-Plas	21) elastic scattering	$H^- + H_2(v) \rightarrow H^- + H_2(v)$
	22) molecular assisted recombination MAR	$e + H_2^+ \rightarrow H(n=1) + H(n=2,3)$
	23) molecular assisted dissociation MAD	$e + H_2^+ \rightarrow e + H^+ + H(n=1)$
	24) molecular assisted ionization MAI	$e + H_2^+ \rightarrow 2e + 2H^+$
	25) electron detachment	$e + H^- \rightarrow 2e + H(n=1)$
Gas-Gas	26) charge exchange recombination	$H^+ + H^- \rightarrow H(n=1) + H(n=2,3)$
	27) atomic elastic scattering	$H(n) + H_2(v) \rightarrow H(n) + H_2(v)$
	28) atomic-induced vibrational excitation VTa	$H(n) + H_2(v) \rightarrow H(n) + H_2(w)$
$H_2$	29) atomic-induced dissociation VTa-diss	$H(n) + H_2(v) \rightarrow H(n) + H(n=1) + H(n=1)$
	30) molecular elastic scattering	$H_2(v) + H_2(w) \rightarrow H_2(v) + H_2(w)$
	31) molecular-induced vibrational excit. VTm	$H_2(v) + H_2(w) \rightarrow H_2(v) + H_2(w')$
	32) molecular-induced dissociation VTm-diss	$H_2(v) + H_2(w) \rightarrow H_2(v) + H(n=1) + H(n=1)$
	33) molecular-induced vibrational exchange VV	$H_2(v) + H_2(w) \rightarrow H_2(v \pm 1) + H_2(w \pm 1)$
	34) molecular-induced vibrational VV-diss	$H_2(v) + H_2(w) \rightarrow H_2(v \pm 1) + H(n=1) + H(n=1)$

**Table II** - List of the most significant surface processes included in the model. W has been considered as divertor plate material.

Colliding particle	Surface Process
electron	<ul style="list-style-type: none"> <li>- absorption <math>1 - \gamma_{\text{see}}</math></li> <li>- reflection <math>\gamma_{\text{see}}</math>: - <math>\eta_{\text{see}}</math>: backscattered electrons</li> <li>- <math>\delta_{\text{see}}</math>: re-difused electrons</li> <li>- <math>\tau_{\text{see}}</math>: true secondary electrons</li> </ul>
atom H/ ion $H^+$	<ul style="list-style-type: none"> <li>- absorption: <math>1 - R</math></li> <li>- reflection: <math>R \rightarrow - R(1 - \gamma_{\text{rec}})</math>: H</li> <li>- <math>R\gamma_{\text{rec}}p_{\text{ER}}</math>: recombinative desorption: ER mechanism: <math>H_2(w)</math></li> <li>- <math>R\gamma_{\text{rec}}p_{\text{LH}}</math>: recombinative desorption: LH mechanism: <math>H_2(w)</math></li> </ul>
molecule $H_2$ / ion $H_2^+$	<ul style="list-style-type: none"> <li>- absorption: <math>1 - R</math></li> <li>- reflection: <math>R \rightarrow - R(1 - \gamma_{\text{diss}})</math>: <math>H_2(v-1)</math></li> <li>- <math>R\gamma_{\text{diss}}</math>: dissociation: <math>H(n=1) + H(n=1)</math></li> </ul>

The investigation was carried out at ASDEX Upgrade conditions for a completely detached plasma phase [3] (plasma density  $n_p = 1 \times 10^{20} \text{ m}^{-3}$  with an electron temperature of  $T_e = 3 \text{ eV}$ ; magnetic field  $B = 1 \text{ T}$  forming an angle  $\theta = 85^\circ$  with the normal to the surface).

The spatial profiles of all plasma and gas species are shown in Fig. 1. Concerning the plasma composition in steady state, we have found peak value of MAR precursors  $H_2^+$  (red line) and  $H^-$  (green line) very close to the divertor wall (0.1 – 0.2 mm). Their density shows a continuous decreasing from about  $1 \times 10^{18} \text{ m}^{-3}$  towards the bulk region due to two different reasons: a) reduction of their production by electron dissociative attachment  $e + H_2 \rightarrow H + H^-$  and atomic-to-molecular ion conversion  $H^+ + H_2 \rightarrow H + H_2^+$  due to the reduction of molecular hydrogen  $H_2$  density and b) enhancement of their destruction by mutual neutralization  $H^- + H^+ \rightarrow H + H$  and dissociative recombination of molecular ions  $H_2^+ + e \rightarrow H + H$  due to the increase of  $H^+$  ion and electron densities, respectively. The ratio between molecular and atomic densities is a clear signature of MAR mechanisms. While the molecular density monotonically decreases from the wall to the bulk region, the atomic density is almost flat and starts decreasing relatively far from the divertor wall. Near the surface the ratio  $n_{H_2}/n_H$  is maximum  $\sim 10$  and decreases reaching its minimum  $\sim 1$  at  $z=1.4 \text{ mm}$  from the divertor plate where the two different MAR mechanisms dominate. Then, the atomic density starts to decrease as well due to ionization of MAR atoms produced  $e + H \rightarrow e + e + H^+$ . This process becomes important as soon as the electron temperature reaches the critical value of  $T_e = 1.8 \text{ eV}$  (see Fig. 2.a).

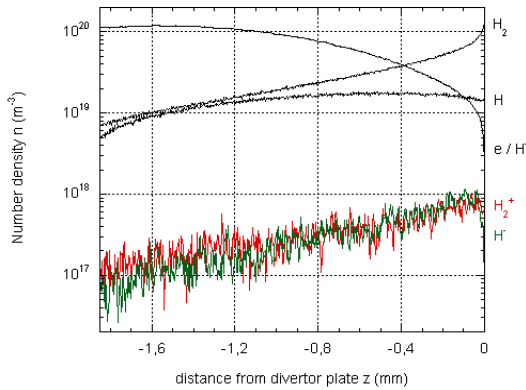


**Fig. 1** - Spatial profile of plasma and gas densities in the divertor region.

In Figs. 2 kinetic temperature profiles of the different plasma and gas species are shown. The electron temperature, which represents one of the leading quantities for estimation of the ratio between atomic (MAR products) ionization and molecular recombination, shows a decreasing from 2 eV in the bulk region to 1 eV at the divertor plate. It never reaches a value smaller than

1 eV, proving the difficulty of EIR mechanisms to happen. The atomic ionization previously discussed occurs in the bulk region ( $z < -1.4$  mm) where the electron temperature is larger than 1.8 eV. The atomic temperature is comparable to  $H^+$  ion temperature due to the ion wall neutralization, which represents the main atomic production mechanism. Nevertheless, atoms result warmer than ions in a region close to divertor wall ( $z > -1.2$  mm). The slight difference between the two temperatures is again a signature of MAR mechanism, in particular of the exothermic molecular ion dissociative recombination  $H_2^+ + e \rightarrow H + H$ . Molecular temperature lies in the range between 0.1–0.3 eV.

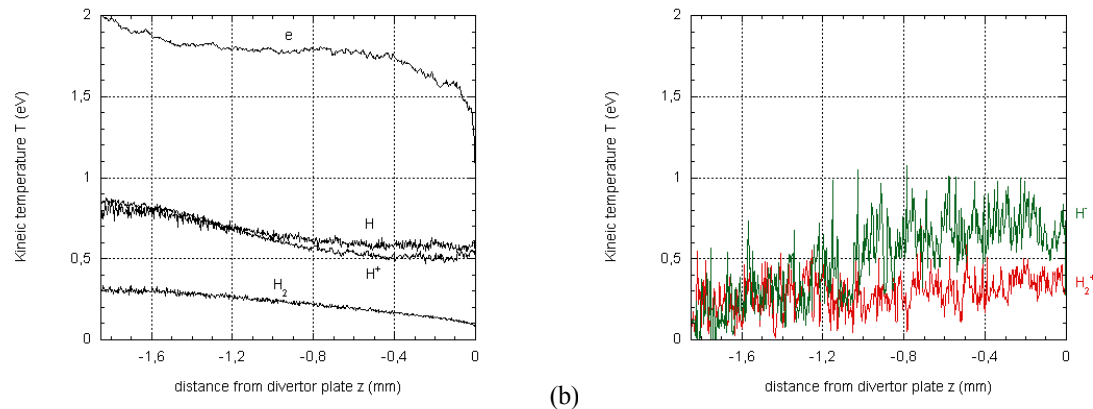


**Fig. 2** - Spatial profile of a) plasma (electron and  $H^+$  ion) and gas ( $H$  and  $H_2$ ) and b) plasma ( $H_2^+$  and  $H^-$  ion) kinetic temperatures in the divertor region.

## References

- [1] G. F. Matthews, J. Nucl. Mater. 220-222 (1995) 104.
- [2] N. Ohno, et al., Phys. Rev. Lett. 81(4) (1998) 818.
- [3] U. Fantz, D. Reiter, B. Heger, D. Coster, J. Nucl. Mat. 290-293 (2001) 367.
- [4] A. Yu. Pigarov, Phys. Scripta T96 (2002) 16.
- [5] K. Sawada, T. Fujimoto, Contrib. Plasma Phys. 42(6-7) (2002) 603.
- [6] K. Miyamoto, A. Fukano, A. Hatayama, Contrib. Plasma Phys. 46(7-9) (2006) 643.
- [7] R. Schneider, et al., Contr. Plasma Phys. 46(1-2) (2006) 3.
- [8] W. M. Stacey, Phys. Plasmas 5(4) (1998) 1015.
- [9] T. Q. Hua, J. N. Brooks, Phys. Plasmas 1(11) (1994) 3607.
- [10] C. K. Birdsall, A. B. Langdon, Plasma Physics via Computer Simulation, (McGraw-Hill, 1985).
- [11] G. A. Bird, Molecular Gas Dynamics and the Direct Simulation of Gas Flows (Oxford Science, 1994).
- [12] F. Taccogna, et al., J. Nucl. Mat. 363-365 (2007) 437.
- [13] F. Taccogna, et al., Contrib. Plasma Phys. 48(1-3) (2008) 147.
- [14] F. Taccogna, P. Minelli, D. Bruno, S. Longo, R. Schneider, to appear on Chem. Phys.